Neutron resonance spectroscopy of ^{104}Pd, ^{105}Pd, and ^{110}Pd

D. A. Smith,[1,*] J. D. Bowman,[1] B. E. Crawford,[2,†] C. A. Grossmann,[3] T. Haseyama,[4,‡] A. Masaike,[4,§] Y. Matsuda,[4,‖] G. E. Mitchell,[3] S. I. Penttila,[1] N. R. Roberson,[2] S. J. Seestrom,[1] E. I. Sharapov,[5] S. L. Stephenson,[3,†] A. M. Sukhovoj,[5] and V. W. Yuan[1]

[1]*Los Alamos National Laboratory, Los Alamos, New Mexico 87545*

[2]*Duke University, Durham, North Carolina 27708*
and Triangle Universities Nuclear Laboratory, Durham, North Carolina 27708-0308

[3]*North Carolina State University, Raleigh, North Carolina 27695-8202*
and Triangle Universities Nuclear Laboratory, Durham, North Carolina 27708-0308

[4]*Physics Department, Kyoto University, Kyoto 606-01, Japan*

[5]*Joint Institute for Nuclear Research, RU-141980 Dubna, Russia*

(Received 25 August 2000; revised manuscript received 30 August 2001; published 16 January 2002)

We have measured neutron resonances in the palladium isotopes 104, 105, and 110 for neutron energies from 1 to 2100 eV. Many new *p*-wave resonances have been observed. Their neutron widths and, in several cases, the radiative widths were measured. The average level spacings and the *s*-wave and *p*-wave neutron strength functions were determined. The time-of-flight method was used for both neutron total cross section measurements and total (n,γ) reaction yield measurements at the pulsed spallation neutron source of Los Alamos Neutron Science Center. Well established resonance spectroscopy for these isotopes is essential for the analysis of parity violation data that were recently measured in palladium.

DOI: 10.1103/PhysRevC.65.024607 PACS number(s): 25.40.Ny, 24.80.+y, 27.60.+j

I. INTRODUCTION

The TRIPLE (time reversal and parity at low energy) Collaboration is studying parity nonconservation (PNC) in neutron resonances [1–3] using the pulsed longitudinally polarized neutron beam at the Los Alamos Neutron Science Center (LANSCE). The PNC effects manifest themselves as parity-odd asymmetries of the *p*-wave resonance neutron cross sections. These asymmetries are due to the mixing of the *p*-wave resonances with nearby *s*-wave resonances through the weak interaction. The goal is to obtain the root-mean-square PNC matrix elements for nuclei over a broad mass region. In order to extract the rms PNC matrix element for a particular nuclide from parity-odd asymmetries, its resonance parameters for both the *s*- and *p*-wave neutron resonances are needed. Although one can average over unknown parameters, this averaging increases the uncertainty in the determination of the PNC matrix elements. Therefore knowledge of the relevant neutron resonance spectroscopy is a prerequisite for the PNC analysis.

Since these experiments require observation of low energy *p*-wave resonances, which are usually weak, the most favorable mass regions are near the $3p$ and $4p$ neutron strength function maxima, $A \simeq 110$ and $A \simeq 240$. For analysis simplicity, one would prefer to study even-mass targets with spin $I=0$. However, the magnitude of the observed PNC effects is proportional to the level density, and the average level density of spin-zero nuclei in the mass region near $A=110$ is low. One can compensate this low density (and smaller PNC effects) by studying odd-mass targets with their higher level densities and larger experimental asymmetries. The price to be paid is a much more complicated analysis, as described by Bowman *et al.* [4].

Palladium is an interesting element for study in the $A \simeq 110$ region, since it has one odd-mass isotope ^{105}Pd and a number of even isotopes in appreciable abundance. All of the primary palladium isotopes are available in high isotopic enrichments. Parity nonconserving asymmetries of the neutron cross sections of palladium have been found in several *p*-wave resonances, as described in a forthcoming paper [5]. However, the low energy neutron cross section data, as compiled by Mughabghab *et al.* [6], have serious limitations for all of the palladium isotopes. Recent tables of neutron resonance parameters compiled by Sukhoruchkin *et al.* [7] complement the earlier information [6] on ^{105}Pd with previously unpublished data of Staveloz *et al.* [8]. We performed spectroscopic measurements on both isotopically enriched and natural palladium targets. Our results for ^{106}Pd and ^{108}Pd were published previously [9]. The present paper reports the spectroscopic results for ^{104}Pd, ^{105}Pd, and ^{110}Pd.

The plan of the paper is as follows. In Sec. II the experimental procedures for the neutron transmission and capture measurements are described. In Sec. III the analysis of the time-of-flight spectra with the fitting code FITXS is presented. In Sec. IV specifics of resonance data for different palladium isotopes are given and the individual resonance parameters are listed in tables. In Sec. V we discuss the orbital angular momentum assignment, the neutron width distributions, and the deduced average resonance parameters. Section VI summarizes the paper.

*Present address: Stanford Linear Accelerator Center, Stanford, CA 94309.

†Present address: Gettysburg College, Gettysburg, PA 17325.

‡Present address: Institute for Chemical Research, Kyoto University, Kyoto 611-0011, Japan.

§Present address: Fukui University of Technology, 3-6-1 Gakuen, Fukui-shi 910-8505, Japan.

‖Present address: Institute of Physical and Chemical Research (RIKEN), Saitama 351-0198, Japan.

II. EXPERIMENTAL PROCEDURES

The experiments were performed at flight path 2 of the LANSCE spallation neutron source [10]. The 800-MeV H^- beam from the LANSCE linac is transported to the proton storage ring (PSR). The negative ion beam is converted to protons by thin foil stripping and injected into the PSR. The injected beam is stacked onto itself until protons from the entire linac macropulse are stored. This reduces the proton pulse width from about 800 μs to about 125 ns full width at half maximum. Then the PSR pulse is extracted and the beam strikes a tungsten target, creating fast neutrons. After passing through a chilled water moderator, the neutrons have a white energy spectrum. The neutron energy was determined from the time of flight over a 59.4-m distance from source to detector. In the present experiment two types of measurements were performed: neutron transmission and neutron capture.

In the neutron transmission experiment the attenuation of the neutron flux through a cylinder of natural palladium metal was measured. This target was a cylinder of 9.1-kg pure palladium metal, of 11.0-cm diameter and an areal density of 5.42×10^{23} atoms/cm^2. The neutron beam was collimated to a 10.4-cm diameter. To reduce Doppler broadening, the target was cooled to liquid nitrogen temperatures. Without this cooling, isotopic identification of the large number of resonances in the transmission spectrum would have been impossible. In the transmission measurement, the neutron resonances were observed as dips in the neutron flux transmitted through the target. With the thick target, many strong resonances absorbed all of the neutrons. To provide accurate measurement of the widths of the strongest resonances, two thin natural palladium targets were used. These targets were foils of 2.84-cm diameter, and 0.25-mm and 1.5-mm thickness, and the measurements were performed at room temperature. To reduce the count rate, the beam was collimated to 1-cm diameter on the thin targets.

The detector used in the transmission measurements was a large array of liquid scintillators which contained 5% by weight of ^{10}B [11]. In order to handle the high instantaneous counting rate, which could be as large as 500 MHz, the detector was divided into 55 cells, each with its own photomultiplier tube (PMT). The analog signals from each PMT were converted to logic pulses by a discriminator located near the detector. These pulses were then transferred over 100-m long

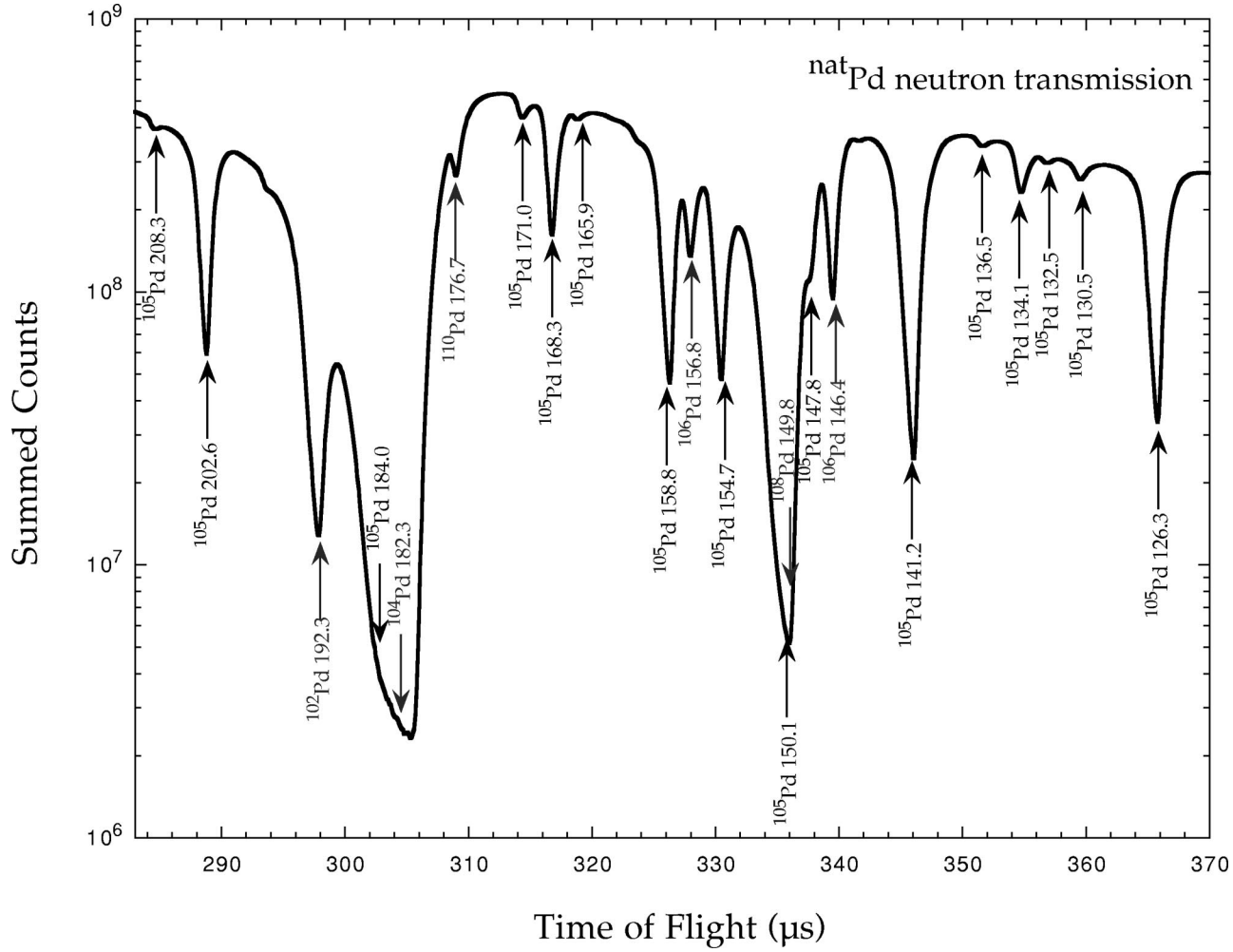

FIG. 1. A section of the neutron time-of-flight spectrum for transmission through the thick target of natural palladium. Neutron counts are plotted vs neutron time of flight.

TABLE I. Isotopic assay for the targets used in the present experiment. The amount of isotope is listed as the percentage of the target material.

	Target					
Isotope	104	105	106[a]	108[a]	110	Natural
102	0.15±0.01	<0.02	<0.02	0.013±0.003	0.014±0.004	1.02
104	95.11±0.05	0.5±0.02	0.16±0.01	0.15±0.01	0.153±0.01	11.14
105	2.7±0.02	97.32±0.05	0.75±0.02	0.34±0.02	0.343±0.01	22.33
106	1.26±0.02	1.72±0.02	98.51±0.05	0.5±0.02	0.464±0.01	27.33
108	0.56±0.01	0.34±0.02	0.45±0.02	98.59±0.05	1.42±0.02	26.46
110	0.21±0.01	0.12±0.01	0.13±0.01	0.42±0.2	97.61±0.04	11.72

[a]Targets used in previous experiment (Ref. [9]).

coaxial cables to the counting house where they were rediscriminated. The 55 signals were linearly summed and shaped to have the same width as the digitization interval. The summed signal voltage was encoded by a transient digitizer for entry into the computer. In this experiment the digitization interval was 100 ns and the number of samples for each beam pulse was 8192. Data were analyzed in the neutron energy range from 30 eV to 1 keV. The digitized time-of-flight spectra were summed and accumulated in the computer. A complete description of the transmission detector is given in Ref. [11]. A typical time-of-flight spectrum measured for neutron transmission is shown in Fig. 1. Most of the resonances are from ^{105}Pd, but there are numerous resonances from the even isotopes. The primary problem in the analysis is illustrated in this spectrum: most of the resonances are from ^{105}Pd, and resonances from other isotopes are observed only if they are very strong or are well separated from the strong resonances in ^{105}Pd.

The second type of measurement performed in this work was neutron capture on isotopically enriched targets of ^{104}Pd, ^{105}Pd, and ^{110}Pd. These spectroscopic measurements were necessary for identifying all resonances appearing in the transmission spectrum of natural palladium and determining their resonance parameters. The thin targets for these measurements were contained in cans made of pure aluminum. Isotopically enriched palladium powders of 4.99 g each were packed into the cans as thin disks of 2.52-cm diameter and 3.15-mm thickness. The isotopic composition of the enriched targets, including the previously measured ^{106}Pd and ^{108}Pd, and of natural palladium, is listed in Table I. Since the neutron beam was collimated to a 2.27-cm diameter, all neutron captures occurred within the enriched metal or the aluminum container.

In the neutron capture experiment the detector [12] was an array of 12 CsI crystal logs (consisting of two crystals each). The detector array surrounded the target and provided an approximately 3.0π solid angle for detecting capture γ rays and had a 20-cm cylindrical hole for the target. The capture target was surrounded by a ^{6}Li-loaded, 5-cm thick, polyethylene insert. This insert absorbed scattered neutrons, but transmitted capture γ rays. The CsI crystals were 15-cm long wedges that form annular rings of 20-cm inner diameter and 40-cm outer diameter. The scintillation light from the CsI crystals was detected by the PMT's. The PMT signals were converted to logic pulses by constant fraction discriminators with a threshold that corresponded to a γ-ray energy of 0.3 MeV. In order to reduce the background a coincidence of two detector signals was required for an event to be recorded. The summed signals after the coincidence unit (a complete description of the γ-detector electronics is given in Ref. [12]) were counted by a multiscaler. The start time of the multiscaler spectrum was triggered from the proton pulse. The multiscaler dwell time (channel width) was set to 100 ns or to 1 μs with a spectrum length of 8192 time-of-flight channels. This produced time-of-flight ranges to 0.8192 ms and to 8.192 ms.

Data were analyzed in the neutron energy region from 30 eV to 2.1 keV for the former dwell time and 1 eV to 300 eV for the latter dwell time. In Fig. 2 typical neutron capture time-of-flight spectra of the isotopically enriched targets and of natural palladium are shown for a time-of-flight region which corresponds to the same energy range as that for the transmission spectrum in Fig. 1. By comparing the spectra from the various targets, isotopic identification of the resonances is performed. Since all of the targets were enriched to greater than 95%, it was a simple matter to make the isotopic assignment for the resonances. In the figure the resonance energy is indicated in the spectrum from which the resonance was identified.

Resonance energy calibrations were performed relative to known resonance energies in ^{105}Pd and ^{110}Pd [6]. The time offset from the beginning of the multiscaler data, which is needed for the energy calibrations, was constant for all data measured during that beam cycle. The time offset and the flight path length for the time-of-flight measurements were determined by fitting peaks to known resonance energies. A flight path length of 59.34±0.02 m was determined for the capture experiment and a flight path length of 56.84 ±0.02 m was obtained for the transmission experiment. The errors on the flight path lengths and time offsets are the dominant systematic errors in the measured energies of the neutron resonances.

III. ANALYSIS WITH FITXS CODE

A. Overview

The time-of-flight spectra were analyzed with the fitting code FITXS [13], which was developed by the TRIPLE Collaboration for analysis of epithermal neutron transmission

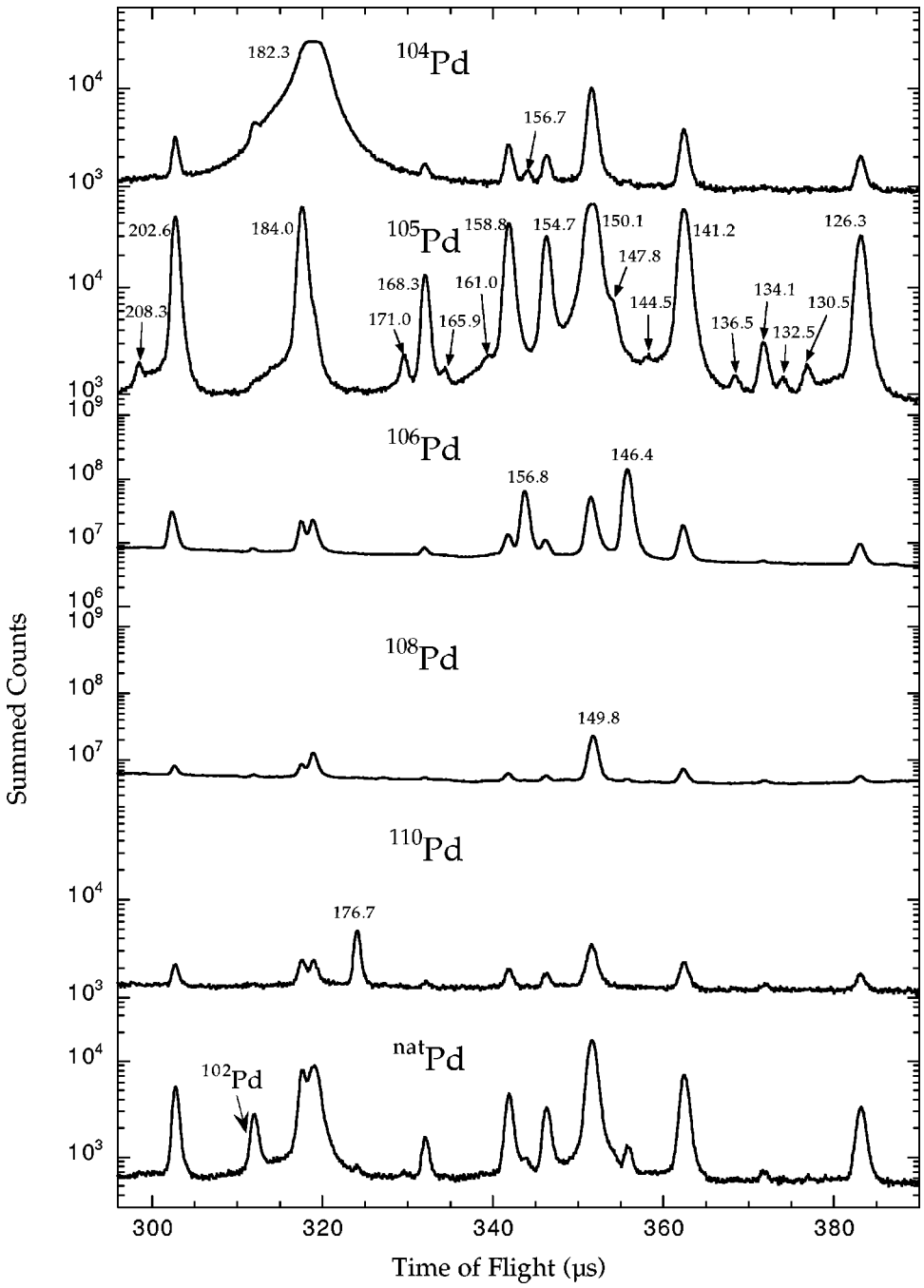

FIG. 2. A section of the neutron time-of-flight spectrum for neutron capture on five isotopically enriched targets and natural palladium. The resonance energies are labeled in the spectrum from which they were identified.

and radiative capture data. In this code, the multilevel, multichannel formalism of Reich and Moore [14] is used to calculate neutron cross sections. The code has also the LANSCE specific response functions including all instrumental resolution effects that are observed in the neutron time-of-flight spectra such as pulse shape produced by the neutron moderator, time response of the detector, channel bin length, target temperature, and Doppler (D) broadening.

With the FITXS code, the standard Breit-Wigner resonance parameters E_0, $g\Gamma_n$, and the total radiative width Γ_γ of the cross section $\sigma_D(E)$ are determined by fitting directly to the data detector count rates versus the time-of-flight channel t. Here g is the standard statistical spin factor $g=(2J+1)/[2(2I+1)]$, with J the resonance spin and I the target spin. The following fitting functions for the transmission (T) and the capture (C) experiments were used:

$$\mathcal{F}_T(t)=N_T(t)\epsilon_T\int[R_T(t')e^{-n\sigma_D(t-t')}]dt'+B_T, \quad (1)$$

$$\mathcal{F}_C(t)=N_C(t)\epsilon_C \times\int\left[R_C(t')\frac{\sigma_D^\gamma(t-t')}{\sigma_D(t-t')}(1-e^{-n\sigma_D(t-t')})\right]dt'+B_C, \quad (2)$$

where $N_T(t)$, $N_C(t)$ and ϵ_T, ϵ_C are the neutron fluxes and

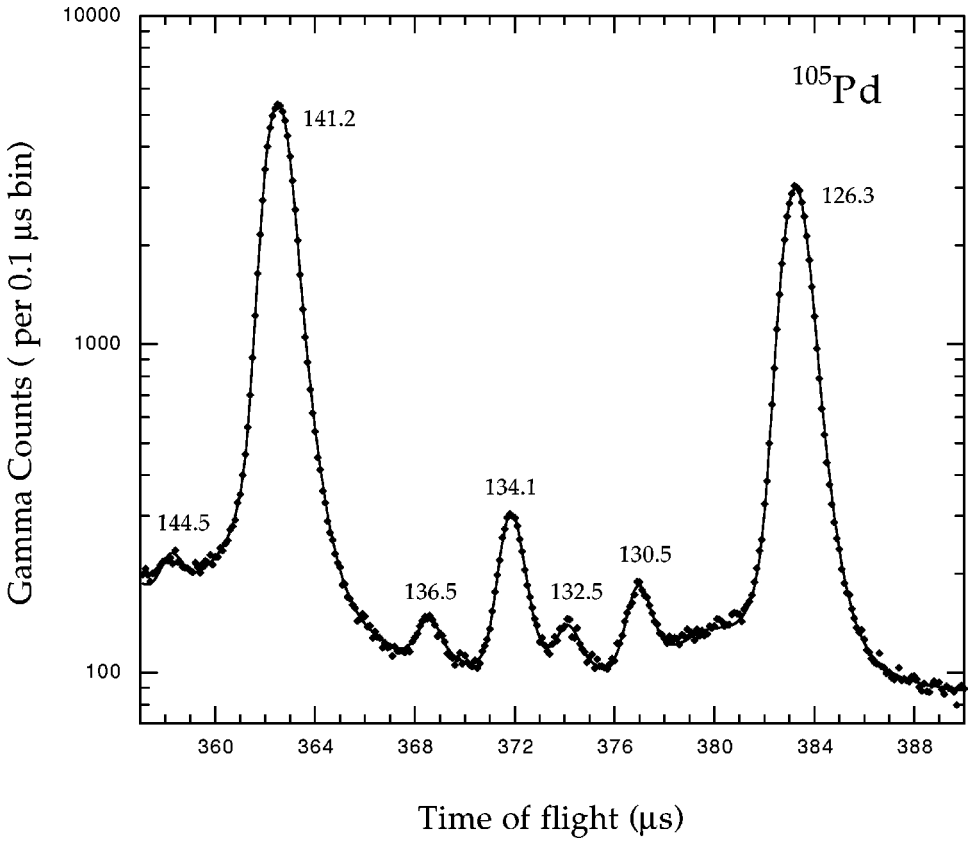

FIG. 3. A sample fit to the neutron capture time-of-flight spectrum in ^{105}Pd. The data are displayed as points and the fit from the code FITXS is the line.

detector efficiencies in the transmission and neutron capture experiments, and B_T and B_C are the corresponding background count rates. The response functions $R_T(t')$ and $R_C(t')$ were parametrized after studying resonances with known intrinsic widths as described in detail by Crawford *et al.* [9] and were input into the FITXS code to be used in the data analysis as discussed in Ref. [15].

A sample fit of the ^{105}Pd capture data for a time-of-flight region near 130 eV is shown in Fig. 3. Counts per 0.1 μs time-of-flight bin are plotted versus time of flight, with the fit to the data shown as a solid line. In this energy range there are five *p*-wave resonances and two much larger *s*-wave resonances in ^{105}Pd. As is clear from the figure, the resonances were fit well with the FITXS code.

B. Neutron flux measurement

With the code FITXS one fits directly to the time-of-flight transmission spectra. The energy dependence of the neutron flux $N_T(E)$ in Eq. (1) was measured in a separate experiment with a well calibrated ^{3}He scintillation detector [16] under the same beam line conditions as were present during the palladium experiment. For a neutron energy between 5 eV and 1500 eV, the flux was shown to follow a power law

$$N(E) = cE^{-p}. \tag{3}$$

The energy dependence of the efficiency for the ^{3}He detector was determined from the detector geometry and the well known $(n,^3\mathrm{He})$ cross section, providing a precise determination of the power law exponent in the neutron flux of $p = 0.960 \pm 0.005$. This result differs from a sum of two exponentials fit to the flux shape of Ref. [17]. However, this earlier measurement was performed at a LANSCE flight path that used neutrons from the ''high intensity'' moderator, while our measurement is for the ''high-resolution'' moderator. The absolute value of the neutron flux (actually the product of the neutron flux and the detector efficiency measured in Ref. [11] as a function of the neutron energy) was then fit to known resonance parameters, resulting in a final error of (5–10)% depending on the accuracy of these resonance parameters. This uncertainty is the dominant error in the measured neutron widths of *p*-wave resonances, since the statistical error is about 0.1%.

Before the normalization was made by fitting to resonance parameters, effects due to material in the beam were included. A sample-out measurement was performed with the 1-cm diameter collimator since the standard 10-cm beam diameter would overload the detector. The thin aluminum windows of evacuated tubes influenced the energy dependence of the flux only in the vicinity of the manganese neutron resonance near 337 eV.

This calibration method was used also for the neutron capture data where it relies on the known resonances parameters in each isotope under study. The complications that we encountered in calibrating the isotopic capture measurements are described below.

C. Analysis of transmission data

With the energy dependence of the neutron flux known, only an overall normalization must be determined from the

data using previously measured resonance parameters. The palladium resonances that were used for calibration are indicated in the tables below. The background in the transmission measurements was determined by using ''black'' neutron resonances at specific energies where the neutrons of a given flight time are completely absorbed. At these energies the detector counts only background neutrons and γ rays. The application of this method with an emphasis on the γ-ray component of the background at the LANSCE flight path 2 is described in detail by Yen *et al.* [18]. Resonances in foils of ^{55}Mn, ^{115}In, ^{181}Ta, ^{113}Cd, and in palladium were used. For the thick natural palladium target, the strong *s*-wave resonances were black for several linewidths above and below the resonance energy. The background rate versus time of flight was fit to a fourth order polynomial and subtracted from the data prior to further analysis.

The resonance energies and neutron widths for strong *s*-wave resonances were initially determined by fitting transmission data measured with thin targets (1.5-mm and 0.25-mm thick foils). These resonance parameters were then used in the subsequent analysis of all resonances in the thick target data. The thick target data were also used to determine the nuclear potential scattering radius R' from the asymmetric shape of the well isolated strong resonances in transmission produced by the interference between the *s*-wave resonance scattering amplitude and the potential scattering amplitude.

D. Analysis of neutron capture data

In principle, the resonance capture data are influenced by a multiple scattering contribution. Numerical simulations of the capture after multiple scattering were performed with a code by Stephenson *et al.* [19]. This code uses the Monte Carlo method to model neutron capture after potential scattering with the cross section σ_{pot} in a realistic sample geometry. A typical size of the multiple scattering correction for this experiment is about (3–5)% relative to the primary resonance capture. The capture samples were small in diameter and thin ($n\sigma_{pot}=0.03$), which explains the small size of the multiscattering contribution. Therefore these multiscattering corrections were neglected for the *p*-wave resonances studied in this experiment. A larger correction could occur if a neutron is captured in a *p*-wave resonance after first scattering in a *s*-wave resonance. However, such an event requires the correct energy spacing ΔE_{sp} between the pair of resonances. The neutron energy loss averaged over all scattering angles is $\Delta E \simeq 2E/A$; only those neutrons that have an energy $E=E_0+\Delta E$ higher than the *p*-wave resonance energy E_0 are effectively captured after scattering. The coincidence of ΔE_{sp} and ΔE occurred for very few cases. For these few *p*-wave resonances we increased the uncertainty of $g\Gamma_n$.

However, for a number of strong *s*-wave resonances multiple scattering did produce an appreciable shoulder on the high energy side. These secondary peaks were input into FITXS as artificial resonances. This procedure minimized the influence of multiple scattering in fitting the *s*-wave resonances.

TABLE II. γ-ray multiplicities and capture detector efficiencies.

Isotope	E_B (MeV)	D_0 (eV)	$\langle M\rangle$	ϵ_c
^{104}Pd	7.0	220±65	4.2±0.1	0.38±0.04
^{105}Pd	9.6	12±1	4.3±0.1	0.60±0.05
^{110}Pd	5.8	275±79	4.2±0.1	0.37±0.04

The capture measurements were performed under the same flight path conditions as for the transmission experiment. Therefore the energy dependence of the flux measured with the ^{3}He detector described above was used in the analysis of the capture data. Because there could be different detector efficiencies for the different isotopes, the value of the product of the efficiency ϵ_C in Eq. (2) and the flux constant *c* in Eq. (3) was determined by fitting the capture detector function of Eq. (2) to known *s*-wave resonance parameters in ^{104}Pd, ^{105}Pd, and ^{110}Pd separately for each isotope. The detection efficiencies obtained differ for the different isotopes. The efficiency values for ^{105}Pd and ^{110}Pd were accepted, since for these isotopes there were several resonances with known parameters that were used in the calibration. However, for ^{104}Pd there was only one resonance that was previously known below 2.7 keV, the strong *s*-wave resonance at 182.3 eV with $\Gamma_n=297\pm4$ MeV and $\Gamma_\gamma=217\pm12$ MeV [6]. Using these parameters for the ^{104}Pd capture calibration led to a ^{104}Pd efficiency about 60% relative to that for ^{105}Pd.

We remeasured the neutron width of the 182.3-eV resonance in transmission with the result 303±9 MeV. Thus the Γ_γ value is crucial for the ^{104}Pd calibration. To ensure that the data normalization on this single resonance was reliable, a calculation of the Pd γ-ray cascades and the detector efficiencies was performed. This followed the approach of Ref. [20]—a Monte Carlo modeling of the γ-ray cascades. With the cascades data in hand and with the known CsI response function, the detector efficiency in the twofold coincidence mode was calculated. For example, for a particular cascade with multiplicity $M=3$, one has

$$\epsilon_c(M=3)=2K(M=3)[\epsilon_\gamma(E_1)\epsilon_\gamma(E_2)+\epsilon_\gamma(E_1)\epsilon_\gamma(E_3)+\epsilon_\gamma(E_2)\epsilon_\gamma(E_3)], \quad (4)$$

where $\epsilon_\gamma(E)$ is the absolute efficiency (with the 0.3-MeV instrumental threshold) of one crystal log for detecting a γ ray of energy *E*, $K(M=3)$ is the number of the CsI log pairs detecting a given cascade (see, e.g., Ref. [12]), and the total energy of the cascade is the neutron binding energy $E_B=E_1+E_2+E_3$. Any other particular cascade with the same multiplicity $M=3$ may have a different distribution of energy between its components, and Eq. (4) takes that into account. All together, contributions from multiplicities up to $M=6$ were included, and the efficiency ϵ_c was obtained as the averaged value over all γ cascades.

The results for the average multiplicity $\langle M\rangle$ and the neutron capture efficiency ϵ_c are listed in Table II together with the values of the neutron binding energy E_B and the *s*-wave level spacing D_0. Calculations were performed for several models of the γ-ray strength function and the level density.

TABLE III. Neutron resonance parameters for ^{102}Pd.

Energy (eV)	l	Bayesian probability	$g\Gamma_n$ (MeV)	Γ_γ (MeV)	$g\Gamma_n^l$ (MeV)
190.7±0.2[a]	0	0.00	269±4	109±16	19.5±0.3
420.5±0.3	0	0.00	333±31		16.2±1.6
800.0±1.0	0	0.29	37±20		1.3±0.7

[a]Resonance parameters from Ref. [6].

Within the limits of the uncertainties listed, the results are insensitive to the model chosen. The error bars on ϵ_c include the uncertainties of the absolute efficiency for detecting a single γ ray. The larger efficiency for registering the neutron capture in the ^{105}Pd isotope is influenced primarily by the higher neutron separation energy. These calculations support our normalization of the ^{104}Pd neutron capture data.

The calculations also were performed for different spins and parities of neutron resonances in palladium. The results were also insensitive to these parameters, which agrees with the conclusion of an experimental study of the detector efficiency for *s*- and *p*-wave resonances in ^{106}Pd and ^{108}Pd by Crawford [21].

E. Radiative widths from transmission and capture data

Resonance shape analysis with good instrumental resolution permits the simultaneous determination of both the $g\Gamma_n$ and Γ_γ widths from one data set. This method requires adequate statistics and a clean line shape (no overlap with nearby resonances). In our palladium data, determining the Γ_γ width from the peak shape could only be performed for a few resonances below neutron energies of about 100 eV. For most of the palladium resonances, the analysis relies essentially on the area of the resonance. In neutron capture measurements the area of the peak is determined by both $g\Gamma_n$ and Γ_γ. When $g\Gamma_n$ is small compared to Γ_γ, the peak area is mainly sensitive to $g\Gamma_n$, and an average value of Γ_γ can

TABLE IV. Neutron resonance parameters for ^{104}Pd.

Energy[a] (eV)	l	Bayesian probability	$g\Gamma_n$ (MeV)	Γ_γ (MeV)	$g\Gamma_n^l$ (MeV)	Footnote
109.73±0.04	1	0.98	0.062±0.006		27.8±2.7	b
156.7±0.1	1	0.98	0.024±0.002		6.1±0.6	c
182.3±0.1	0	0.00	297±4	217±12	22.0±0.3	d
266.6±0.1	1	0.96	1.07±0.10		126±12	b
294.5±0.1	1	0.95	1.30±0.13		132±13	e
347.3±0.2	0	0.11	15.7±1.5		0.8±0.1	f
522.0±0.4	1	0.95	4.3±0.4		186±18	c
524.4±0.4	1	0.95	2.0±0.2		84±8	c
607.5±0.5	1	0.93	4.5±0.5		152±17	c
638.7±0.5	1	0.90	7.8±0.8		247±25	c
678.9±0.4	1	0.95	2.4±0.3		70±9	b
738.2±0.5	1	0.95	2.7±0.3		70±8	b
769.2±0.7	1	0.96	0.21±0.02		4.8±0.5	c
888.1±0.8	1	0.92	7.2±0.7		141±14	c
935.0±0.8	1	0.88	13.0±1.2		235±22	c
944.5±0.6	0	0.00	700±65		23±2	f
994.9±0.9	0	0.63	35.0±3.2		1.2±0.1	c
1176±1	1	0.95	0.8±0.3		9.9±3.8	c
1189±1	0	0.00	>900		>26	c
1314±1	0	0.40	70.0±6.0		1.9±0.2	c
1334±1	1	0.85	25.0±2.8		259±29	c
1454±2	1	0.92	11.1±1.0		102±10	c
1480±2	1	0.86	27.0±2.9		243±25	c
1522±2	0	0.55	70.3±6.5		1.8±0.2	c
1847±2	1	0.92	12.2±1.1		79±7	c
1871±2	1	0.92	9.8±1.0		63±6	c
2000±2	1	0.93	2.0±0.9		17±8	c
2031±2	0	0.00	>900		>20	c

[a]All resonances are new except for the 182.3-eV resonance (Ref. [6]).
[b]Data from thick target transmission and capture.
[c]Data from neutron capture only.
[d]Resonance used for data normalization.
[e]Data from thin and thick target transmission and capture.
[f]Data from thin target transmission and capture.

TABLE V. Neutron resonance parameters for ^{105}Pd.

Energy (eV)	J^a	l	Bayesian probability	$g\Gamma_n$ (MeV)	Γ_γ (MeV)	$g\Gamma_n^l$ (MeV)	Footnote
-6.07^a	3	0			(177)	0.95	
3.912 ± 0.004^b		1	0.97	$0.000\,46\pm0.000\,03$	146 ± 7	30.4 ± 1.7	c
11.780 ± 0.007	3	0	0.00	0.105 ± 0.001	150 ± 2	0.031 ± 0.0006	d
13.222 ± 0.007	2	0	0.00	1.33 ± 0.05	163 ± 7	0.37 ± 0.01	e
24.49 ± 0.02^b		0	0.00	0.080 ± 0.005		0.016 ± 0.001	e
25.09 ± 0.01	3	0	0.00	1.79 ± 0.05	151 ± 6	0.36 ± 0.01	e
27.59 ± 0.04^b		1	0.97	0.0032 ± 0.0003		11.3 ± 1.1	c
30.05 ± 0.02	2	0	0.00	0.180 ± 0.002	152 ± 4	0.033 ± 0.0003	d
38.43 ± 0.02	3	0	0.00	0.189 ± 0.009	158 ± 8	0.030 ± 0.002	e
41.16 ± 0.02^b		1	0.97	0.0053 ± 0.0002	158 ± 23	10.2 ± 0.4	f
42.56 ± 0.02		0	0.57	0.033 ± 0.001	159 ± 14	0.0051 ± 0.0002	f
44.37 ± 0.02^b		1	0.96	0.0079 ± 0.0003	122 ± 24	13.7 ± 0.6	f
49.93 ± 0.02^b		1	0.98	0.0021 ± 0.0001		3.0 ± 0.1	f
55.23 ± 0.02	3	0	0.00	3.9 ± 0.1	158 ± 11	0.53 ± 0.01	g
68.27 ± 0.02	3	0	0.00	0.92 ± 0.03	159 ± 17	0.112 ± 0.004	g
72.51 ± 0.03^b		1	0.96	0.0139 ± 0.0006		11.5 ± 0.5	f
77.72 ± 0.03	2	0	0.00	7.8 ± 0.2	152 ± 11	0.88 ± 0.03	g
79.47 ± 0.03^b		1	0.96	0.0139 ± 0.0007		10.0 ± 0.5	f
80.45 ± 0.03^b		1	0.91	0.033 ± 0.001		23.6 ± 1.0	f
82.90 ± 0.03^b		1	0.92	0.032 ± 0.001		21.6 ± 1.0	f
83.30 ± 0.03^b		1	0.90	0.039 ± 0.002		26.4 ± 1.2	f
86.74 ± 0.03	3	0	0.00	10.2 ± 0.3	158 ± 16	1.10 ± 0.03	g
94.29 ± 0.06^b		1	0.97	0.0076 ± 0.0008		4.2 ± 0.4	c
101.19 ± 0.04		1	0.94	0.028 ± 0.001		14.0 ± 0.6	f
104.01 ± 0.04	3	0	0.00	0.72 ± 0.03	155 ± 15	0.071 ± 0.003	g
113.45 ± 0.07^b		1	0.97	0.0071 ± 0.0009		3.0 ± 0.4	c
116.93 ± 0.05		1	0.94	0.036 ± 0.002		14.7 ± 0.6	f
126.27 ± 0.05	3	0	0.00	1.88 ± 0.06	147 ± 15	0.168 ± 0.006	g
130.44 ± 0.05		1	0.93	0.044 ± 0.002		15.1 ± 0.6	f
132.49 ± 0.05^b		1	0.95	0.025 ± 0.001		8.4 ± 0.4	f
134.08 ± 0.05		1	0.74	0.122 ± 0.005		40.3 ± 1.7	f
136.47 ± 0.06		1	0.95	0.026 ± 0.001		8.3 ± 0.4	f
141.17 ± 0.05	2	0	0.00	5.75 ± 0.50	157 ± 5	0.48 ± 0.04	d
144.48 ± 0.06^b		1	0.96	0.0192 ± 0.0009		5.7 ± 0.3	f
147.82 ± 0.06^b		1	0.87	0.158 ± 0.007		45.0 ± 1.9	f
150.07 ± 0.05	2	0	0.00	32.6 ± 1.0	150 ± 11	2.66 ± 0.08	g
154.68 ± 0.06	3	0	0.00	2.07 ± 0.08	179 ± 27	0.167 ± 0.006	g
158.76 ± 0.06	2	0	0.00	3.5 ± 0.1	171 ± 26	0.279 ± 0.009	g
160.97 ± 0.07^b		1	0.96	0.026 ± 0.001		6.5 ± 0.3	f
165.88 ± 0.07^b		1	0.95	0.040 ± 0.002		9.6 ± 0.4	f
168.28 ± 0.08	3	0	0.04	0.87 ± 0.04	134 ± 20	0.067 ± 0.003	g
171.00 ± 0.09		1	0.91	0.082 ± 0.004		18.8 ± 0.9	f
183.98 ± 0.09	2	0	0.00	7.7 ± 0.4		0.57 ± 0.03	e
202.6 ± 0.1	2	0	0.00	5.6 ± 0.2	160 ± 24	0.39 ± 0.01	g
208.3 ± 0.1		1	0.94	0.057 ± 0.002		9.7 ± 0.4	f
215.5 ± 0.1		1	0.91	0.103 ± 0.004		16.6 ± 0.7	f
222.7 ± 0.1^b		1	0.94	0.049 ± 0.002		7.5 ± 0.3	f
226.8 ± 0.1	3	0	0.00	4.0 ± 0.1	147 ± 22	0.27 ± 0.01	g
230.4 ± 0.1^b		1	0.94	0.050 ± 0.002		7.4 ± 0.4	f
251.4 ± 0.1	2	0	0.00	3.0 ± 0.1		0.190 ± 0.008	g
252.4 ± 0.1	3	0	0.00	19.80 ± 0.25	25	1.25 ± 0.05	d
260.0 ± 0.1	2	0	0.00	22.4 ± 0.7	153 ± 23	1.39 ± 0.05	g
268.4 ± 0.1^b		1	0.91	0.116 ± 0.005		13.5 ± 0.6	f

TABLE V. (*Continued*).

Energy (eV)	J^a	l	Bayesian probability	$g\Gamma_n$ (MeV)	Γ_γ (MeV)	$g\Gamma_n^l$ (MeV)	Footnote
284.6±0.2		1	0.84	0.23±0.02		24.5±1.9	e
286.8±0.3	3	0	0.00	3.15±0.10		0.185±0.005	d
300.3±0.2[b]		1	0.95	0.016±0.003		1.6±0.3	c
305.1±0.2	2	0	0.00	53.3±1.7	124±19	3.1±0.1	c
311.0±0.2[b]		1	0.94	0.057±0.003		5.3±0.3	g
313.3±0.2	2	0	0.05	2.05±0.09		0.116±0.005	h
322.1±0.2[b]		1	0.94	0.072±0.003		6.3±0.3	f
327.7±0.2	3	0	0.00	1.7±0.1		0.095±0.005	d
328.4±0.2[b]		1	0.93	0.088±0.004	160±32	7.6±0.4	f
339.4±0.2		1	0.87	0.23±0.01		18.8±0.8	f
344.1±0.2[b]		1	0.93	0.108±0.005		8.6±0.4	f
346.9±0.2		0	0.00	32.0±1.5		1.7±0.1	d
349.0±0.2[b]		0	0.10	1.06±0.04		0.057±0.002	f
354.0±0.2	3	0	0.00	34.1±1.1		1.81±0.06	f
365.2±0.2[b]		1	0.92	0.150±0.007		11.0±0.5	g
370.1±0.2	2	0	0.00	11.1±0.4		0.58±0.02	f
376.9±0.2	2	0	0.02	3.0±0.1		0.157±0.007	g
384.2±0.2[b]		1	0.90	0.206±0.009		14.0±0.6	f
388.6±0.2	3	0	0.00	12.3±0.5		0.63±0.02	f
392.5±0.2		1	0.78	0.43±0.04		28.4±2.4	g
394.4±0.2		1	0.90	0.211±0.010		13.8±0.6	c
401.1±0.3	3	0	0.01	3.7±0.2		0.186±0.008	f
411.6±0.3		1	0.80	0.43±0.03		26.5±2.1	f
417.6±0.3		0	0.01	2.12±0.09		0.104±0.004	c
430.8±0.3	2	0	0.00	35.1±1.9	129±26	1.69±0.09	f
448.9±0.3	3	0	0.00	25.2±1.0		1.19±0.04	e
461.2±0.3[b]		1	0.90	0.25±0.02		12.8±1.1	g
466.0±0.3	2	0	0.00	66.7±2.2		3.1±0.1	c
476.6±0.3[b]		1	0.87	0.34±0.01		16.9±0.7	g
481.3±0.3		0	0.10	3.3±0.2		0.149±0.007	f
491.6±0.3		1	0.89	0.28±0.01		13.2±0.6	f
498.2±0.3		1	0.93	0.133±0.006		6.1±0.3	f
510.8±0.3		0	0.17	1.62±0.07		0.072±0.003	f
512.3±0.3		0	0.50	1.04±0.04		0.046±0.002	f
523.0±0.4[b]		1	0.93	0.11±0.02		4.9±0.7	f
525.4±0.4[b]		1	0.91	0.22±0.02		9.2±0.9	c
531.2±0.4	3	0	0.00	14.8±0.5		0.64±0.02	d
537.8±0.4[b]		1	0.93	0.067±0.003		2.8±0.1	f
545.9±0.4		0	0.00	48.9±1.9		2.09±0.08	f
556.6±0.4[b]		1	0.92	0.15±0.02		6.0±0.8	g
566.2±0.4		0	0.00	11.7±0.6		0.49±0.02	c
575.8±0.4	3	0	0.00	9.2±0.5		0.38±0.02	h
588.8±0.4[b]		0	0.52	1.23±0.06		0.051±0.003	h
589.6±0.5	3	0	0.00	51.8±2.6		2.1±0.1	i
592.8±0.5	2	0	0.00	18.0±0.8		0.74±0.04	d
603.4±0.5	3	0	0.00	48.9±2.0		1.99±0.08	h
609.4±0.5		1	0.74	0.83±0.04		28.2±1.4	i
614.5±0.5		0	0.01	3.4±0.2		0.137±0.007	h
619.0±0.5	3	0	0.00	22.2±1.1		0.89±0.04	h
656.4±0.5		(1)	0.69	1.02±0.05		31.1±1.6	i
660.9±0.5	2	0	0.00	33.2±1.4		1.29±0.06	h
667.8±0.5		1	0.81	0.70±0.03		20.7±1.0	i

TABLE V. (*Continued*).

Energy (eV)	J^a	l	Bayesian probability	$g\Gamma_n$ (MeV)	Γ_γ (MeV)	$g\Gamma_n^l$ (MeV)	Footnote
676.2±0.5		1	0.86	0.51±0.03		14.8±0.7	h
680.1±0.6		0	0.02	3.7±0.2		0.142±0.007	h
694.3±0.6	3	0	0.00	16.2±0.8		0.62±0.03	h
697.6±0.6	2	0	0.00	11.0±0.6		0.42±0.02	h
710.2±0.6	3	0	0.00	60.5±2.5		2.27±0.09	h
721.7±0.6	3	0	0.00	26.4±1.3		0.98±0.05	i
731.2±0.6		(0)	0.65	1.30±0.07		0.048±0.003	h
735.9±0.6		(1)	0.69	1.2±0.1		30.2±2.6	h
747.7±0.6		0	0.01	5.2±0.3		0.189±0.009	h
754.5±0.6	3	0	0.00	32.8±1.6		1.20±0.06	h
776.9±0.7	3	0	0.00	55.0±2.8		1.97±0.10	h
785.9±0.7	2	0	0.00	24.3±1.2		0.87±0.04	h
791.2±0.7	3	0	0.00	24.3±1.2		0.87±0.04	h
804.1±0.7	2	0	0.00	12.0±0.6		0.42±0.02	h

[a]Data from Ref. [6].
[b]New resonance measured in this work.
[c]Data from neutron capture only.
[d]Resonance from Ref. [6] used for data normalization.
[e]Data from thin target transmission and capture.
[f]Data from thick target transmission and capture.
[g]Data from thin and thick target transmission and capture.
[h]Data from thin target transmission only.
[i]Data from thin and thick target transmission.

be used in fitting the resonance. If $g\Gamma_n$ is stronger there are problems in determining its value from a single capture experiment and often the neutron width cannot be determined from the capture data alone. Qualitatively this is clear from the expression for the limiting case of a thin sample:

$$\frac{1}{A_\gamma} = \frac{1}{g\Gamma_n} + \frac{1}{g\Gamma_\gamma}, \tag{5}$$

where A_γ is the measured normalized capture area. For small neutron widths the first term in Eq. (5) dominates. When the neutron width exceeds the value of about one tenth of the radiative width, accuracy is lost in the determination of $g\Gamma_n$ from the capture data alone. However, transmission data taken on targets with different thicknesses permit the determination of $g\Gamma_n$ in such cases. The capture data may then be used to determine Γ_γ for resonances of even isotopes (with $g=1$) and for *s*-wave resonances of ^{105}Pd with known spin (most of them are known below 500 eV [6]). This procedure provided determination of new values of Γ_γ for several palladium resonances.

IV. INDIVIDUAL RESONANCE PARAMETERS

Our experimental goal was to determine the resonance parameters for the many new resonances observed in the palladium isotopes, and to use this information in the analysis of parity violation in the *p*-wave resonances. The analysis method that we adopted involves normalization to known resonance parameters, and limits the accuracy in determining the neutron widths at the level of (7–12)%, depending on the precision of the available information. This level of accuracy is adequate for the analysis of the parity violation data on *p*-wave resonances in palladium. The resulting resonance parameters are listed in Tables III—VIII. In these tables, the resonances that were used for data normalization are marked. For resonances for which Γ_γ is not listed, the neutron width was determined using the average radiative width for the particular nuclide, as given in Table IX.

The transmission data on the thick natural palladium target shows neutron resonances in all of the palladium isotopes, while the capture data on isotopically enriched targets provide information on resonances in ^{104}Pd, ^{105}Pd, and ^{110}Pd. In addition, we used results of our earlier measurements on isotopically enriched ^{106}Pd and ^{108}Pd targets performed with both the neutron capture and transmission methods [9].

The presence of several isotopes led to overlapping resonances in the natural palladium transmission spectra. Weak resonances were much better observed in the capture spectra, since the number of overlapping resonances was greatly reduced in the isotopically enriched targets. Even when resonances overlapped, the resonance parameters could be determined in the enriched targets because of the differing isotopic abundances. The measurements that were used in order to determine the resonance parameters are listed in the

TABLE VI. Neutron resonance parameters for ^{106}Pd.

Energy (eV)	l	Bayesian probability	$g\Gamma_n$ (MeV)	Γ_γ (MeV)	$g\Gamma_n^l$ (MeV)	
63.47±0.03	1	0.99	0.0132±0.0006	107±12	13.3±0.6	a
146.37±0.05	1	0.96	0.60±0.03	97±7	172.0±7.2	a
156.88±0.06	1	0.98	0.25±0.02	107±8	70.1±5.6	b
281.5±0.2	0	0.00	515±14	73±20	30.7±0.8	c
299.8±0.2	1	0.98	0.24±0.01		23.7±1.1	c
406.4±0.2	1	0.97	0.83±0.03		51.4±1.8	a
461.9±0.2	1	0.96	1.16±0.04		59.4±2.0	a
521.9±0.4	1	0.89	6.0±0.3		256±13	d
562.5±0.3	1	0.91	5.5±0.2		209±8	a
593.4±0.5	(1)	0.75	12.0±0.4		419±15	a
644.9±0.6	1	0.97	0.52±0.05		16.1±1.6	d
870.6±0.6	0	0.00	877±30		29.7±1.0	e
921.4±0.6	0	0.00	705±26		23.2±0.8	e
967.5±0.6	1	0.85	16±1		274±17	f
1005.3±0.7	0	0.11	58±4		1.83±0.13	f
1147.9±0.9	1	0.95	4.0±0.4		52±5	f
1206.2±0.9	1	0.925	10.0±0.7		122±9	f
1306±1	1	0.95	3.4±0.3		37±3	f
1323±1	1	0.93	7.8±0.8		82±8	f
1377±1	1	0.95	2.2±0.2		22±2	f
1398±2	0	0.00	231±17		6.2±0.5	f
1511±2	1	0.84	28±2		243±17	f
1557±2	1	0.95	1.7±0.2		14±2	f
1585±3	0	0.02	153±12		3.8±0.3	f
1597±2	1	0.92	12±1		96±8	f
1624±2	1	0.93	10±1		78±8	f
1764±2	1	0.91	18±2		124±14	f
1839±4	0	0.00	914±67		21±2	f

[a]Data from thick target transmission and capture.
[b]Resonance used for data normalization.
[c]Data from thin and thick target transmission and capture.
[d]Data from neutron capture only.
[e]Data from thin target transmission only.
[f]Data from Ref. [9].

tables. If the parameters were determined in several measurements, then the average value is listed. If a resonance with a sizeable neutron width was not observed in both transmission and capture spectra, then usually the neutron and γ-ray widths could not be separately determined.

As the analysis was extended to higher energies, the resonance parameters became much more uncertain due to poorer resolution. The highest energies included in the analysis are different for the different isotopes.

In a few cases there were resonances in the ^{104}Pd neutron capture spectrum that were stronger in the natural palladium spectrum. These were *s*-wave resonances in ^{102}Pd. No isotopically enriched target of ^{102}Pd was studied. Even for the thick transmission target used, no *p*-wave resonances in ^{102}Pd were observed: the sensitivity of transmission measurements with the natural target (1% abundance of ^{102}Pd) was too low to perform neutron spectroscopy for *p*-wave resonances in ^{102}Pd. Of the three ^{102}Pd *s*-wave resonances listed in Table III one was known previously. Our result for its neutron width, $\Gamma_n = 257 \pm 9$ MeV, agrees with the more precise value listed in Table III that is taken from Ref. [6].

For ^{104}Pd only one resonance at 182.3 eV was known previously in this energy range. All of the other information listed was determined in the present experiment. Although the analysis was extended up to 2 keV, the uncertainties in the resonance parameters for the higher energy resonances are substantially larger. For the strong 1189-eV and 2031-eV resonances only a lower limit on the neutron width could be determined. However, the higher energy resonances were valuable in determining the level densities. The resonance parameters are listed in Table IV.

In ^{105}Pd the resonance density is high, and many new weak resonances were observed. Because of the small level spacing it is very difficult to separate the resonances at higher energies. For ^{105}Pd the higher energy resonances are not crucial, since the parity violation study was only performed up to 400 eV. The lower energy data are sufficient to determine the relevant average resonance parameters. Analy-

TABLE VII. Neutron resonance parameters for ^{108}Pd.

Energy (eV)	l	Bayesian probability	$g\Gamma_n$ (MeV)	Γ_γ (MeV)	$g\Gamma_n^l$ (MeV)	Footnote
32.98±0.01	0	0.00	123±4	95±6	21.3±0.6	a
90.98±0.04	0	0.00	214±6	91±12	22.4±0.6	a
112.70±0.06	1	0.83	0.98±0.06	114±10	422±15	b
149.76±0.07	1	0.99	0.060±0.006		16.4±1.6	c
302.7±0.1	1	0.84	3.7±0.1	102±5	349±14	d
410.6±0.2	1	0.97	0.69±0.02		42±1	d
426.6±0.2	0	0.00	371±11		18.0±0.5	a
480.3±0.3	1	0.97	0.62±0.02		29.8±1.1	d
544.4±0.4	1	0.90	5.6±0.3		221±12	c
634.5±0.3	0	0.00	396±12		15.7±0.5	a
642.2±0.6	1	0.97	1.3±0.1		40±3	c
797.4±0.8	1	0.93	6.3±0.4		141±9	c
842.8±0.6	1	0.97	1.3±0.1		26.8±1.3	d
904.0±0.6	0	0.00	585±29		19.5±1.0	c
954.6±0.6	0	0.00	877±37		28.4±1.2	e
962.4±1.0	0	0.12	47.1±0.4		1.52±0.01	f
1082.3±0.8	1	0.85	17±1		240±14	f
1121±2	1	0.97	0.51±0.05		6.8±0.7	f
1140±2	1	0.97	0.08±0.02		1.0±0.3	f
1215±2	0	0.00	418±42		12.0±1.2	f
1359±1	1	0.80	28±2		281±20	f
1433±2	0	0.00	148±15		3.9±0.4	f
1456±1	1	0.95	4.5±0.5		41±5	f
1505±2	1	0.96	0.33±0.05		2.8±0.4	f
1523±2	1	0.96	2.8±0.3		24±3	f
1652±3	0	0.00	1269±127		31±3	f
1710±3	0	0.37	77±8		5.9±0.6	f
1743±2	1	0.95	0.47±0.07		3.2±0.5	f
1815±2	1	0.95	2.4±0.2		15.6±1.3	f
2010±4	0	0.00	696±70		15.5±1.6	f
2118±3	1	0.94	7.5±0.8		39±4	f
2165±3	1	0.95	2.6±0.3		13.0±1.5	f
2287±4	1	0.87	37±4		170±1	f

[a]Data from thin and thick target transmission and capture.
[b]Resonance used for data normalization.
[c]Data from neutron capture only.
[d]Data from thick target transmission and capture.
[e]Data from thin target transmission only.
[f]Data from Ref. [9].

sis of the capture data was performed up to 575 eV, and analysis of the transmission data up to 800 eV. The resonance parameters determined in these energy ranges are listed in Table V. Note that our neutron widths for the resonances at 430.8 eV and 545.9 eV are of one order of magnitude smaller than the values reported in Ref. [6]. These misprints are corrected in the recent compilation [7].

Resonance parameters for ^{106}Pd and ^{108}Pd were published previously by Crawford *et al.* [9]. In order to provide a complete set of resonance parameters for all of the palladium isotopes in one place, we also include the results for ^{106}Pd and ^{108}Pd in Tables VI and VII. The present transmission results for low energy resonances were combined with those from Ref. [9], which led to an increased accuracy for the parameters of some resonances below ~900 eV.

The results for ^{110}Pd are listed in Table VIII. Several new resonances were observed up to 500 eV, although the data are far from complete. Since no PNC effects were observed in this nuclide, the data for ^{110}Pd are not needed for our parity violation analysis.

V. AVERAGE RESONANCE PARAMETERS

A. Orbital angular momentum assignment

After the neutron resonance parameters were determined, the probability that a resonance was *s* wave or *p* wave was

TABLE VIII. Neutron resonance parameters for ^{110}Pd.

Energy (eV)	l	Bayesian probability	$g\Gamma_n$ (MeV)	Γ_γ (MeV)	$g\Gamma_n^l$ (MeV)	Footnote
-20.0[a]	0			(60)	0.29	
5.190 ± 0.004[b]	1	0.99	0.0024 ± 0.0001		100 ± 4	c
71.00 ± 0.06[b]	1	0.98	0.0026 ± 0.0004		2.15 ± 0.33	c
86.23 ± 0.05	1	0.93	0.47 ± 0.03	108 ± 16	290 ± 19	c
134.0 ± 0.1[b]	1	0.98	0.007 ± 0.001		2.2 ± 0.3	c
176.64 ± 0.07	1	0.96	0.32 ± 0.01	88 ± 18	67.5 ± 2.1	d
262.7 ± 0.1	0	0.57	5.5 ± 0.3		0.34 ± 0.02	e
392.1 ± 0.3[b]	1	0.96	0.037 ± 0.008		2.36 ± 0.51	c
422.1 ± 0.4[b]	1	0.96	0.028 ± 0.009		1.6 ± 0.5	c
552.2 ± 0.3	1	0.89	4.7 ± 0.3		187 ± 12	e
578.4 ± 0.4	1	0.95	0.61 ± 0.05		21.7 ± 1.8	c
636.5 ± 0.4	1	0.95	0.710.06		21.9 ± 1.9	e
734.5 ± 0.6	1	0.94	1.5 ± 0.1		37.3 ± 2.5	c
857.2 ± 0.7	0	0.68	22 ± 1		0.75 ± 0.04	c
898.0 ± 0.6	0	0.00	193 ± 21		6.44 ± 0.70	f
953.9 ± 0.9	1	0.90	6.6 ± 0.5		111 ± 9	c
957.6 ± 0.9	1	0.84	13.9 ± 0.8		232 ± 13	c
1003.6 ± 0.9	0	0.20	56 ± 4		1.76 ± 0.13	c
1173.4 ± 1.1	(0)	0.74	28 ± 2		0.77 ± 0.06	c
1320.2 ± 1.3	1	0.92	17 ± 1		175 ± 10	c
1427.8 ± 1.5	1	0.91	5.3 ± 0.4		48.6 ± 4	c
1605.9 ± 1.5[a]	1	0.88	15.4 ± 1.2		110 ± 9	
1664.6 ± 1.5[a]	0	0.00	961 ± 24	57.4 ± 4.0	23.6 ± 0.6	
1693.6 ± 1.5[a]	1	0.85	23.2 ± 5.7		165 ± 40	

[a]Data from Ref. [6].
[b]New resonance measured in this work.
[c]Data from neutron capture only.
[d]Data from thick target target transmission and capture.
[e]Resonance used for data normalization.
[f]Data from thin and thick target transmission and capture.

estimated with a Bayesian analysis developed by Bollinger and Thomas [22]. This analysis makes use of the average resonance parameters and assumes that the neutron reduced widths obey the Porter-Thomas distribution. At low neutron energies, because of the large difference in penetrabilities for *s*-wave and *p*-wave resonances, most of the stronger resonances are *s* wave and the weaker resonances are *p* wave. Using the notation of Ref. [9], the probability of a resonance being *p* wave is

$$BP=\left\{1+\frac{\pi_s}{\pi_p}\sqrt{\frac{3\pi_s S_1 c^0(E)}{\pi_p S_0 c^1(E)}}\times\exp\left[-\frac{g\Gamma_n c^0(E)}{2D_0}\left(\frac{1}{S_0}-\frac{\pi_p c^1(E)}{3\pi_s S_1 c^0(E)}\right)\right]\right\}^{-1}, \tag{6}$$

TABLE IX. Average resonance parameters for palladium isotopes.

Isotope	R' (fm)	$\langle\Gamma_{\gamma0}\rangle$ (MeV)	$\langle\Gamma_{\gamma1}\rangle$ (MeV)	D_0 (eV)	D_1 (eV)	S_0 (10^{-4})	S_1 (10^{-4})
^{104}Pd	6.7 ± 0.4	217 ± 12		220 ± 65	74 ± 14	0.47 ± 0.24	4.5 ± 1.6
^{105}Pd		157 ± 16	148 ± 16	12 ± 1		0.55 ± 0.15	4.4 ± 1.0
^{106}Pd[a]	6.5 ± 0.3	73 ± 20	102 ± 9	217 ± 61	85 ± 19	0.6 ± 0.3	4.0 ± 1.0
^{108}Pd[a]	6.9 ± 0.3	94 ± 9	104 ± 8	182 ± 33	95 ± 24	0.9 ± 0.4	4.0 ± 1.0
^{110}Pd		(60)[b]	98 ± 17	275 ± 79	76 ± 17	0.2 ± 0.1	3.7 ± 1.5

[a]Results from previous experiment (Ref. [9]), except for R' values.
[b]Data from Ref. [6].

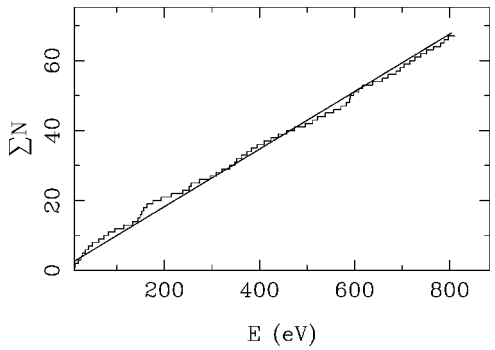

FIG. 4. Cumulative number of *s*-wave resonances in ^{105}Pd. The line is a linear fit to the data below 800 eV.

where π_s/π_p is the ratio of *s*- and *p*-wave level densities, S_0 and S_1 are the *s*- and *p*-wave strength functions, D_0 is the average *s*-wave level spacing, and $g\Gamma_n$ is the neutron width of the state in question. A resonance was assumed to be *p* wave if the Bayesian probability *P* was greater than the *a priori* probability.

To clarify this choice, we remind that the Bayesian conditional probability is defined as

$$BP(l=1|g\Gamma_n)=\frac{P_1*P(g\Gamma_n|l=1)}{P_1*P(g\Gamma_n|l=1)+P_0*P(g\Gamma_n|l=0)}, \tag{7}$$

where P_0 and P_1 are *a priori* probabilities for the resonance to be *s* or *p* wave and $P(g\Gamma_n|l=0)$ and $P(g\Gamma_n|l=1)$ are the Porter-Thomas probabilities for a given $g\Gamma_n$ value and $l=0$ or 1. With a $(2J+1)$ dependence for the level densities, one expects twice as many *p*-wave resonances as *s*-wave resonances for all targets with *I* larger than 1/2. For $I=0$ targets one expects three times as many *p*-wave resonances as *s*-wave resonances. The value of *BP* that results when the Porter-Thomas probabilities for *s*- and *p*-wave choices are equal is taken as the *a priori* probability value that divides *s*-wave and *p*-wave resonances. For the present case this is 66.7% for ^{105}Pd and 75.0% for the even Pd isotopes. Of course the assignment is less reliable when the probability is close to the *a priori* value. The orbital assignment for such cases is noted by parentheses.

The functions $c^l(E)$ in Eq. (6) are

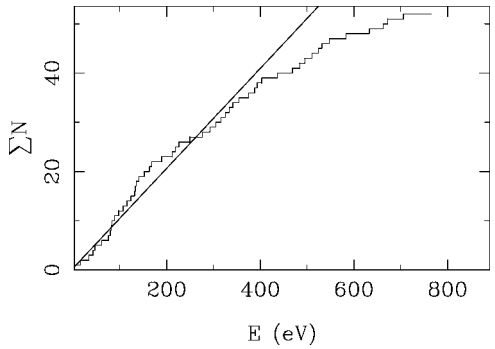

FIG. 5. Cumulative number of *p*-wave resonances in ^{105}Pd. The line is a linear fit to the data below 400 eV.

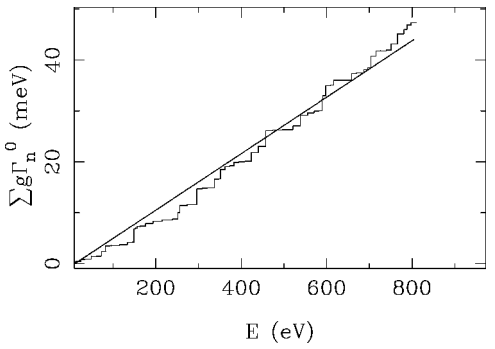

FIG. 6. Cumulative neutron reduced widths for ^{105}Pd *s*-wave resonances. The line is a linear fit to the data below 800 eV.

$$c^l(E)=\frac{[1+(kR)^{2l}]}{(kR)^{2l}\sqrt{E(\mathrm{eV})}}, \tag{8}$$

where the nuclear radius is assumed to be $R=1.35A^{1/3}$ fm. We distinguish between the nuclear radius *R* and the effective radius of the potential scattering R' which appears in Table IX. The probabilities depend on the *s*- and *p*-wave strength functions, and with the $(2J+1)$ assumption, only on the average spacing of the *s*-wave levels. The strength functions were determined by summing the reduced widths over an energy range

$$S_l=\frac{1}{(2l+1)\Delta E}\sum g\Gamma_n^l \tag{9}$$

and the reduced widths were calculated as [6]

$$g\Gamma_n^l=c^l(E)g\Gamma_n. \tag{10}$$

The process of assigning the orbital angular momentum value to resonances with this probabilistic argument, and then determining the strength functions and level densities, was iterated until the probabilities were stable. The final values for the strength functions and average level spacings were insensitive to the change of one or two resonance assignments. The final (Bayesian) probabilities are listed in Tables IV through VIII.

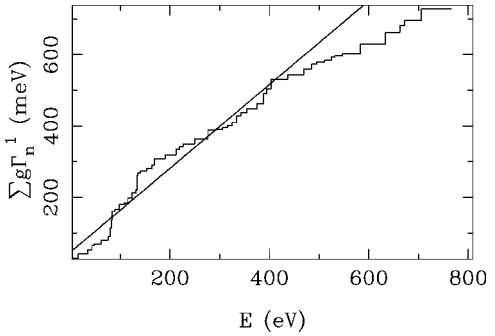

FIG. 7. Cumulative neutron reduced widths for ^{105}Pd *p*-wave resonances. The line is a linear fit to the data below 400 eV.

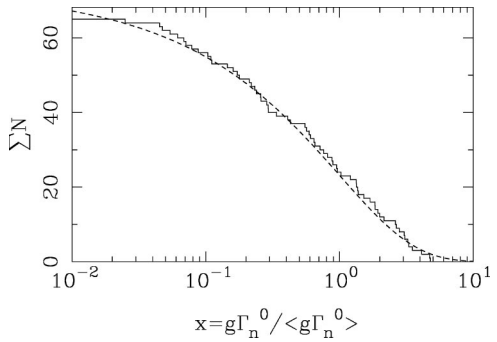

FIG. 8. Cumulative neutron reduced width distribution for *s*-wave resonances in ^{105}Pd compared to the Porter-Thomas distribution.

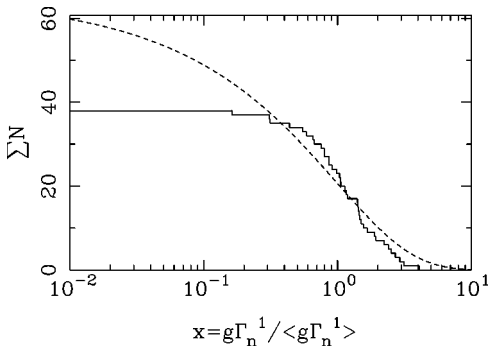

FIG. 9. Cumulative neutron reduced width distribution for *p*-wave resonances below 400 eV in ^{105}Pd compared to the Porter-Thomas distribution.

B. Average parameters D_l, S_l, $\Gamma_{\gamma l}$, and R'

The average resonance parameters: level densities D_l, strength functions S_l, average radiative widths $\Gamma_{\gamma l}$, and the potential scattering radius R' are listed in Table IX. The accuracy of D_l and S_l is limited by the number of resonances studied. The $\Gamma_{\gamma l}$ values are taken as the weighted averages, however the uncertainties given in $\Gamma_{\gamma l}$ propagate from the individual resonance uncertainties. The parameter R' is deduced only for those isotopes which had very strong and well separated resonances in the thick transmission target of natural palladium.

In ^{104}Pd only eight *s*-wave resonances and 20 *p*-wave resonances were observed below 2000 eV, which accounts for the large uncertainties in D_l and S_l. The strength functions and level spacings for ^{106}Pd and ^{108}Pd that were determined by Crawford *et al.* [9] are listed in this table for completeness. For the even nuclide ^{110}Pd, there are only six *s*-wave resonances, which leads to the estimates of D_0 and S_0 listed in Table IX. The resulting *s*-wave strength function value is low compared to other nuclei in this mass region [6], however, due to the very small number of resonances it is rather uncertain. The 14 *p*-wave resonances below 1173 eV, listed in Table VIII, are again insufficient for detailed analysis.

There are sufficient resonances in ^{105}Pd to justify a more detailed examination. In Fig. 4 the cumulative number of *s*-wave resonances in ^{105}Pd is plotted vs energy. The *s*-wave cumulative number follows a straight line, although only on average. The observed *s*-wave level spacing $D_0=12$ eV. There are unusually large local fluctuations in the cumulative number plot. The nearest neighbor spacing distribution for the *s*-wave resonances does not agree with the expected two-Gaussian orthogonal ensemble (GOE) sequence distribution for two spins. These anomalies suggest that further studies of ^{105}Pd are in order—high-resolution measurements at higher neutron energies.

In Fig. 5 the cumulative number of *p*-wave resonances in ^{105}Pd is plotted vs energy. The histogram clearly falls below the line starting at 400 eV. Even in this region the observed number of *p*-wave levels is about the same as the number of *s*-wave levels, indicating a large number of missing *p*-wave levels, which prevents the determination of the average *p*-wave level spacing. For ^{105}Pd the cumulative reduced neutron width vs energy is plotted for the *s*-wave and *p*-wave resonances in Figs. 6 and 7 with the corresponding linear fits yielding the strength functions listed in Table IX.

C. Neutron width distributions

The even isotopes of palladium have relatively large level spacings and do not have many resonances within the measured energy range. Therefore statistical tests were performed only for ^{105}Pd. The distribution of the neutron reduced widths is expected to agree with the Porter-Thomas distribution [6,23],

$$P(x)=\frac{e^{-x/2}}{\sqrt{2\pi x}}, \tag{11}$$

where $x=g\Gamma_n^l/\langle g\Gamma_n^l\rangle$. In Figs. 8 and 9 the cumulative neutron reduced width distributions in ^{105}Pd for *s*- and *p*-wave resonances are compared with the integral of the Porter-Thomas distribution. Since states of smaller size are more likely to be missed, the integral of the distribution is shown from larger to smaller values. The normalization constant of the Porter-Thomas distribution—the total number of levels—was obtained by fitting the distribution to the histogram in the interval $0.2<x<5.0$, where the missing strength should be minimal. The total number of levels under the Porter-Thomas curve extended to $x=0$ is 8% larger than the number of levels above the $x=10^{-2}$ cutoff shown in the figures. Comparison with the histograms indicates that about 9% of the *s*-wave resonances were missed below 800 eV, and that about 40% of the *p*-wave resonances were missed below 400 eV.

VI. SUMMARY

Neutron and radiative widths have been measured for ^{104}Pd, ^{105}Pd, and ^{110}Pd. A transmission measurement with a liquid scintillation detector was performed on a thick natural palladium target and on two thin natural palladium targets. Isotopically enriched targets of ^{104}Pd, ^{105}Pd, and ^{110}Pd were studied in the neutron capture measurement with an array of CsI detectors. The combination of these and previous measurements on ^{106}Pd and ^{108}Pd permitted isotopic

identification of all of the palladium resonances observed.

Many new *p*-wave resonances were observed, especially in ^{104}Pd and ^{105}Pd. The data fitting was performed with the shape analysis code FITXS and neutron widths were obtained for all of the resonances as well as many radiative widths. The orbital angular momentum assignments were made with a Bayesian analysis. Neutron strength functions and level densities were determined for both the *s*- and *p*-wave resonances and are consistent with earlier measurements. This spectroscopic information is very important for extracting the weak interaction matrix elements from recently performed parity violation measurements on palladium isotopes.

ACKNOWLEDGMENTS

This work was supported in part by the U.S. Department of Energy, Office of High Energy and Nuclear Physics, under Grant Nos. DE-FG02-97-ER41042 and DE-FG02-97-ER41033, and by the U.S. Department of Energy, Office of Energy Research, under Contract No. W-7405-ENG-36.

[1] J. D. Bowman, G. T. Garvey, Mikkel B. Johnson, and G. E. Mitchell, Annu. Rev. Nucl. Part. Sci. **43**, 829 (1993).
[2] C. M. Frankle, S. J. Seestrom, Yu. P. Popov, E. I. Sharapov, and N. R. Roberson, Phys. Part. Nucl. **24**, 401 (1993).
[3] G. E. Mitchell, J. D. Bowman, and H. A. Weidenmüller, Rev. Mod. Phys. **71**, 435 (1999).
[4] J. D. Bowman, L. Y. Lowie, G. E. Mitchell, E. I. Sharapov, and Yi-Fen Yen, Phys. Rev. C **53**, 285 (1996).
[5] D. A. Smith *et al.*, Phys. Rev. C (to be published).
[6] S. F. Mughabghab, M. Divadeenam, and N. E. Holden, *Neutron Cross Sections* (Academic, New York, 1981), Vol. 1, Pt. A.
[7] S. I. Sukhoruchkin, Z. N. Soroko, and V. V. Deriglazov, in *Numerical Data and Functional Relationships in Science and Technology*, Landolt-Börnstein, New Series, Group 1, Vol. 16, Pt. b, Low Energy Neutron Physics, Tables of Neutron Resonance Parameters, edited by H. Schopper (Springer, New York, 1998).
[8] P. Staveloz, E. Cornelis, L. Mewissen, F. Poortmans, G. Rohr, R. Shelly, and T. van der Veen, in *Nuclear Cross Sections for Technology*, edited by J. L. Fowler, C. H. Johnson, and C. D. Bowman (National Bureau of Standards Special Publication 594, Washington, D.C., 1980), p. 315.
[9] B. E. Crawford *et al.*, Phys. Rev. C **58**, 729 (1998).
[10] P. W. Lisowski, C. D. Bowman, G. J. Russell, and S. A. Wender, Nucl. Sci. Eng. **106**, 208 (1990).
[11] Yi-Fen Yen *et al.*, Nucl. Instrum. Methods Phys. Res. A **447**, 476 (2000).
[12] S. J. Seestrom *et al.*, Nucl. Instrum. Methods Phys. Res. A **433**, 603 (1999).
[13] J. D. Bowman, Y. Matsuda, Y.-F. Yen, and B.E. Crawford (unpublished).
[14] C. W. Reich and M. S. Moore, Phys. Rev. **111**, 929 (1958).
[15] B. E. Crawford *et al.*, Phys. Rev. C **58**, 1225 (1998).
[16] D. R. Rich *et al.*, e-print archive /physics/9908050, Los Alamos, New Mexico, 1999.
[17] P. Koehler, Nucl. Instrum. Methods Phys. Res. A **292**, 541 (1990).
[18] Yi-Fen Yen *et al.*, Nucl. Instrum. Methods Phys. Res. A **397**, 365 (1997).
[19] S. L. Stephenson, J. D. Bowman, S. J. Seestrom, H. Postma, and E. I. Sharapov, *IV International Seminar on Interactions of Neutrons with Nuclei*, Report No. E3-96-336 (Joint Institute of Nuclear Research, Dubna, 1997), p. 171.
[20] A. M. Sukhovoj and V. A. Khitrov, Yad. Fiz. **62**, 24 (1999) [Phys. At. Nucl. **62**, 19 (1999)].
[21] B. E. Crawford, Ph.D. thesis, Duke University, 1997.
[22] L. M. Bollinger and G. E. Thomas, Phys. Rev. **171**, 1293 (1968).
[23] C. E. Porter and G. E. Thomas, Phys. Rev. **104**, 483 (1956).